Toward eco-friendly dye-sensitized solar cells: Developing chitosan-based electrolytes with conducting polymers and ionic liquids

Adhi Dwi Hatmanto* ⓘ, Indah Puspitaningrum, Yoan Nikita Christina Tefa, Sri Juari Santosa ⓘ, Indriana Kartini ⓘ

Department of Chemistry, Faculty of Mathematics and Natural Sciences, Universitas Gadjah Mada, Yogyakarta, 55281, Indonesia

Abstract. Optimization of chitosan-based gel electrolytes modified with conducting polymers and ionic liquids for dye-sensitized solar cells (DSSC) has been done to improve its electrochemical activity. The effects of iodide salts, 1-propyl-3-methylimidazolium iodide (PMII), and polyaniline incorporation on the electrochemical properties of chitosan-based electrolyte, as well as its performance as a quasi-solid electrolyte in DSSC, were systematically investigated. A study on the effect of different iodide salts on the electrochemical properties of the electrolyte was conducted by employing various iodide salts (lithium iodide, sodium iodide, potassium iodide, or cesium iodide). Electrolytes with various amounts of PMII and polyaniline were also prepared. X-ray diffraction (XRD) and Fourier transform-infrared (FTIR) analysis were conducted to study the effect of iodide salts, PMII, and polyaniline on the change in intermolecular interaction of the chitosan matrix. The ionic conductivity and the redox activity of the chitosan-based electrolyte were respectively evaluated using conductometry and cyclic voltammetry analysis. It is found that the larger cation size of the iodide salts and a higher amount of PMII resulted in both higher intensity of the redox peak current and conductivity of the electrolyte. Those two characteristics increase with the presence of polyaniline, but the low transparency of this polyaniline-based electrolyte lowers the solar cell's efficiency. The highest performance DSSC utilizing a chitosan/KI-PMII based electrolyte resulted in a Voc of 0.402 V, Jsc of 0.335 mA/cm², fill factor (FF) of 0.432, and an overall power conversion efficiency (PCE) of 0.058%. This efficiency is approximately one-third that of the conventional liquid electrolyte-based DSSC. The optimized chitosan-based electrolyte offers promising performance in replacing the low-stability liquid electrolyte-based DSSC.

Keywords: DSSC, chitosan, electrolyte, polyaniline, ionic liquid

1. Introduction

Dye-sensitized solar cells (DSSC), first reported by O'Regan and Gratzel in 1991, have been attracting much attention due to their low cost, easy preparation procedure, and high efficiency (Huang *et al.* 2021, Tamilselvan and Shanmugan 2024). DSSC based on organic liquid electrolytes has achieved a high efficiency of about 14% (Green *et al.* 2017, Zhang *et al.* 2018). However, crucial problems such as electrolyte leakage, solvent evaporation, and instability limit the performance of DSSC for long-term use (Theerthagiri *et al.* 2016, Yahya *et al.* 2017, Gossen *et al.* 2022). Researchers have done some studies to solve these problems, such as replacing liquid electrolytes with polymer electrolytes, which could be prepared in solid (film) or quasi-solid state (gel) systems. The issues in the solid-state systems due to the absence of solvents are the crystallization of the iodide salt, thus lowering the ionic conductivity, and a relatively poor ability to penetrate the TiO2 films as the working electrode (Lai *et al.* 2017). Then, the quasi-solid-state electrolyte offered better electrochemical performance and excellent stability for long-term use (Tang *et al.* 2012).

Polymer-based electrolyte systems consist of a polymer as a matrix, dissolved in a specific solvent, and an ionic compound

to conduct electricity. The use of a polymer-based electrolyte system using polymethylmethacrylate (Dissanayake *et al.* 2014), polyvinylidene-fluoride (PVdF) (Arof *et al.* 2014, Kusumawati *et al.* 2024), and polyacrylonitrile (PAN) (Adel *et al.* 2019) has been demonstrated. Polymer electrolytes could also be formed using blends of different polymers, as reported by Prabakaran *et al.* (Prabakaran *et al.* 2015). The use of some synthetic polymers showed a high stability DSSC but caused relatively high fabrication costs and environmental problems. Some natural polymers have been demonstrated as a matrix for electrolytes in quasi-solid and solid-state DSSC systems. Chitosan is a widely used natural polymer because of its excellent properties: biodegradable, biocompatible, high mechanical strength, non-toxic, chelation, and metal complexation ability (Li *et al.* 2020, Liu *et al.* 2022).

Ionic liquids have been employed in DSSC systems due to their specific properties, such as non-volatile, non-flammable, and high conductivity. Ionic liquids exhibit good solubility in polysaccharide and bio-macromolecule systems (Polesca *et al.* 2022, Mahmood *et al.* 2022). The electrolyte's conductivity and conversion efficiency of DSSC could be enhanced with ionic liquids incorporation (Kitazawa *et al.* 2018, Bandara *et al.* 2019). The use of chitosan-based electrolyte containing 1-ethyl 3-

* Corresponding author
Email: adhi.dwi.h@ugm.ac.id (A.D.Hatmanto)

A.D.Hatmanto et al

Int. J. Renew. Energy Dev 2025, 14(4), 727-739

| 728

methylimidazolium thiocyanate (EMImSCN) (Singh *et al.* 2010), 1-butyl-3-methylimidazolium iodide (BMII) (Buraidah *et al.* 2010), as well as 1-methyl-3-propylimidazolium iodide (PMII) (Yahya *et al.* 2017) ionic liquids as redox mediator in DSSC has been reported. However, its effect on different iodide salts as sources of I^-/I_3^- redox couple has not been investigated yet. In DSSCs, study of the effect of ionic liquids on different iodide salts as sources of the I^-/I_3^- redox pair is crucial because it affects the kinetics of oxidation-reduction process, ionic mobility, as well as overall power conversion efficiency of the device. Specifically, the interaction between ionic liquids and iodide salts used as I^-/I_3^- redox pair can affect the mobility of redox species, rates of recombination, and electrolyte's stability. Understanding these effects is crucial for optimizing electrolyte formulations to enhance the overall conversion efficiency of DSSC. Furthermore, the performance of polymer-based electrolytes could also be enhanced using conducting polymers, including polyaniline and polypyrrole (Lemos *et al.* 2020, Manikandan *et al.* 2018). Polyaniline is one of the widely used conducting polymers due to its high conductivity, stability, and absorbent ability for liquid electrolytes (Lozkins *et al.* 2019, Vimala and Cindrella 2022). Polyaniline plays a crucial role in dye-sensitized solar cells because of its high electrical conductivity that facilitates rapid electron transfer to the electrolyte. This condition is beneficial for regeneration of the I^-/I_3^- redox couple. In addition, polyaniline offer good catalytic activity, mechanical flexibility, low cost, and simple synthesis process, making it attractive for improving the performance and stability of DSSCs. Synergistic role of polyaniline and ionic liquids is expected to result in high performance and stability chitosan-based electrolytes.

In this study, we designed and optimized an eco-friendly quasi-solid electrolyte containing chitosan biopolymer, ionic liquid PMII, alkali iodide salts, and polyaniline. We systematically investigated the effects of different iodide salts (LiI, NaI, KI, and CsI) and electrolyte composition on conductivity and redox behavior, particularly on the intensity of the redox current as well as its reversibility. DSSCs were then fabricated using N719 as dyes, TiO$_2$-coated ITO glass as working electrode, Pt-coated ITO glass as counter electrode, and the chitosan-based gel electrolyte containing PMII, polyaniline, various iodide salts, and iodine (I$_2$) as the redox mediator. The correlation between the electrolyte's electrochemical properties and DSSC performance was thoroughly analyzed. We believed this is the first comprehensive electrochemical study of chitosan-based gel electrolytes exploring the synergistic roles of iodide salts, PMII, and polyaniline.

2. Materials and methods

2.1 Materials

Chitosan (degree of deacetylation: 97%, molecular weight: 298 kDa) was purchased from Biotech Surindo, while lithium iodide (LiI, purity: ≥98.0%), sodium iodide (NaI, purity: ≥99.5%), potassium iodide (KI, purity: ≥99.5%), cesium iodide (CsI, purity: ≥99.5%), iodine (I$_2$, purity: ≥99.8%), acetic acid (CH$_3$COOH, glacial 100%), hydrochloric acid fuming 37% (HCl 37%), ethanol (absolute for analysis, purity: ≥99.9%) , aniline (purity: ≥99.5%), ammonium persulfate (APS, purity: ≥98.0%), and acetonitrile (purity: ≥99.9%) were purchased from Merck. TiO$_2$-coated test cell glass electrode (active area: 0.5 cm × 0.5 cm), platinum-coated test cell counter electrode, 1-methyl-3-propylimidazolium iodide (PMII), and di-tetrabutylammonium cis-bis(isothiocyanato)bis(2,2′-bipyridyl-4,4′-dicarboxylato) ruthenium(II) (N719 dyes) were obtained from Dyesol.

2.2 Methods

2.2.1. Preparation of electrolytes with various iodide salts

Chitosan (2 g) was dissolved in 50 mL of 1% acetic acid solution. Separately, the I^-/I_3^- redox pair were then prepared by dissolving 3.012 mmol of iodide salts (LiI, NaI, KI, and CsI) and 0.3012 mmol of I$_2$ in 50 mL of 1% acetic acid solution. Those two solutions were mixed thoroughly and heated at 60 °C for 6 h. Note that a 10:1 ratio of iodide (I$^-$) to iodine (I$_2$) is commonly used to maintain an efficient redox balance and enhance overall cell performance (Wang *et al.* 2013, Senevirathne *et al.* 2016). This excess of I$^-$ ensures rapid dye regeneration and effective reduction of I$_3^-$, thereby facilitating continuous electron flow and minimizing charge recombination.

2.2.2. Preparation of electrolytes with the addition of ionic liquids.

A chitosan solution was prepared using the same method mentioned before. The I^-/I_3^- redox pair was prepared by dissolving various compositions of KI, PMII, and I$_2$ (as shown in

Table 1
Various compositions of electrolytes (Mass of I$_2$ = 95.6 mg)

Mol percentage (%)		Mass (mg)	
KI	PMII	KI	PMII
100	0	625	0
95	5	594	47
90	10	562	95
85	15	531	142
80	20	500	190

Table 2
Various compositions of polymer matrix

Polymer mass percentage (%)		Mass (g)	
chitosan	polyaniline	chitosan	polyaniline
100	0	2.0	0.0
90	10	1.8	0.2
80	20	1.6	0.4
70	30	1.4	0.6
60	40	1.2	0.8

A.D.Hatmanto et al   Int. J. Renew. Energy Dev 2025, 14(4), 727-739

| 729

Table 1) in 50 mL of a 1% acetic acid solution. Both solutions were mixed thoroughly and heated at 60 °C for 6 h.

2.2.3. Preparation of electrolytes with the addition of conducting polymer.

Ammonium persulfate (3.05 g) was dissolved in 15 mL of 1 M HCl. In a separate step, 1 mL of aniline was mixed with 15 mL of 1 M HCl and stirred for 20 min. The APS solution was then added dropwise to the aniline solution, with the pH remained neutral. The mixture was then stirred for 60 min, covered with aluminum foil and left in the dark for 24 hrs. The resulting polyaniline precipitate (dark green) was collected by filtration, rinsed with 30 mL of deionized water, dried at 65 °C, and finally ground into a fine powder. Then, chitosan and polyaniline (as shown in Table 2) were dissolved in 50 mL of 1% acetic acid solution with continous stirring for 1 h. Electrolyte solutions were prepared by dissolving a certain amount of KI, PMII, and I_2 in 50 mL of 1% acetic. Both solutions were mixed and heated at 60 °C for 6 h.

2.2.4. Fabrication of DSSC.

DSSC was fabricated using TiO_2/dye and Pt as the working electrode and counter electrode, respectively. The dye was prepared by dissolving 0.3 mM of N719 in ethanol. TiO_2-coated test cell glass electrode with an active area of 0.75 cm² was heated at 100 °C for 30 min and then immersed slowly into N719 dye. Gel electrolytes with the highest performance from each study were used as redox electrolytes. The Pt-coated test cell was used as the counter electrode.

2.3 Data Analysis

Electrolyte's redox behavior of electrolytes was evaluated by cyclic voltammetry (Metrohm μ-AutolabIII/FRA2 Potentiostat) using Pt as both working and counter electrodes, and Ag/AgCl as reference, measured at 100 mV/s scan rate. The electrolyte's conductivity of was determined using a Lutron YK-22CT conductivity meter. The functional group of the chitosan electrolyte and its interaction with the iodide salts were investigated using Shimadzu FTIR-Prestige 21 and Shimadzu XRD-6000. The electronic spectra of the dyes were determined using Shimadzu 1800 UV-Vis spectrophotometer. The morphology of chitosan and polyaniline was analyzed using SEM (Thermo Scientific Phenom ProX G6 Desktop). The

photovoltaic performance (J-V curve) of the DSSC was evaluated using a Keithley 2400 with simulated solar illumination of 100 mW/cm².

3. Results and Discussion

Electrochemical activity of chitosan-based gel electrolytes was evaluated using cyclic voltammetry. Figure 1(a) shows the cyclic voltammograms of gel electrolytes with different iodide salts. The anodic peak is related to the oxidation of I^- (reaction 1), while the cathodic peak is attributable to the reduction of I_3^- (reaction 2). In the cyclic voltammetry tests, we performed up to five cycles to assess reproducibility. However, as the analysis results showed no significant variation across cycles, possibly due to the stable electrolyte and electrode surface, the curve presented in this study is representative of the first cycle.

$$\text{Oxidation: } 3I^- \rightarrow I_3^- + 2e \qquad (1)$$

$$\text{Reduction: } I_3^- + 2e \rightarrow 3I^- \qquad (2)$$

Gel electrolytes containing chitosan and various iodide salts show good redox activity due to their high-intensity peaks in both anodic and cathodic areas. As indicated, Figure 1(a) shows two oxidation peaks. The first oxidation was observed at around -0.48 V, which can be assigned to the electrochemical activity of solvents. The second oxidation peak was observed in the 0.89 – 0.96 V range, attributed to the oxidation of I^-. Only one peak in the cathodic area was observed from -0.01 V to -0.03 V, which attributed to the reduction of I_3^-.

Figure 1(b) shows the effects of iodide salts on the anodic and cathodic peak current intensity. We assume that all salts completely dissociate into their ionic components when dissolved in a solvent and penetrate the polymer matrix, so the charge carriers are relatively similar. Therefore, the effect of different iodide salts on the electrochemical properties is only caused by the size of the cation. The sizes of Li^+, Na^+, K^+, and Cs^+ are respectively 0.76 Å; 1.02 Å; 1.38 Å; and 1.67 Å (Bhattacharya et al. 2009). Figure 1(b) confirmed that the anodic and cathodic peak current intensity increased with increasing size of the alkali cation. The effects of cation sizes on the amorphousness of the polymer-based electrolyte systems have been reported (Bhattacharya et al. 2009, Kaneto et al. 2018), stating that the increment of the cation size resulted in the decrease of crystallinity. Higher electrolyte's conductivity is
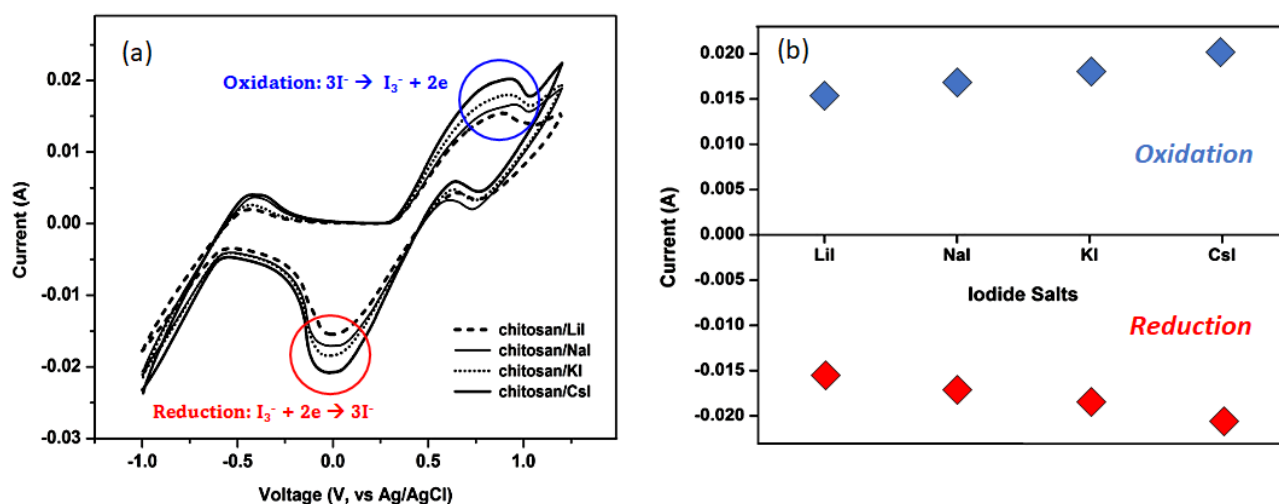
Fig 1. (a) Cyclic voltammograms of gel electrolytes prepared using various iodide salts and (b) effects of iodide salts on the anodic and cathodic peak current
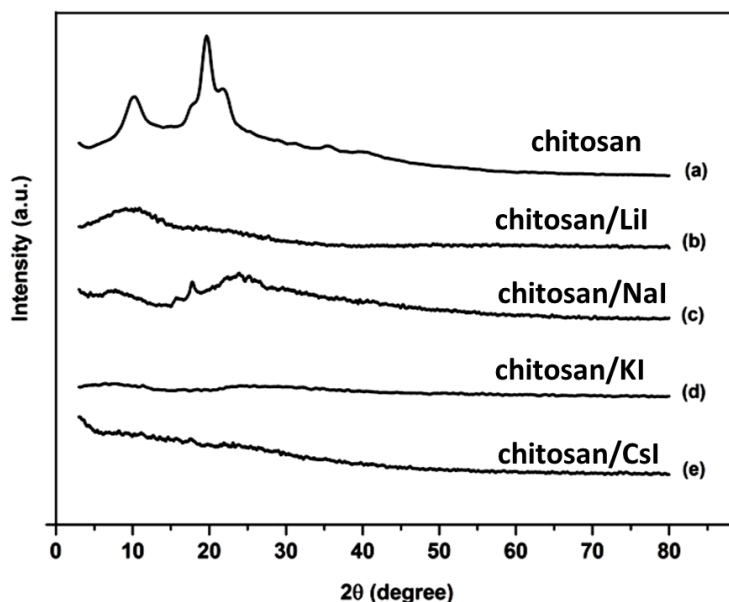
A.D.Hatmanto et al   Int. J. Renew. Energy Dev 2025, 14(4), 727-739

730
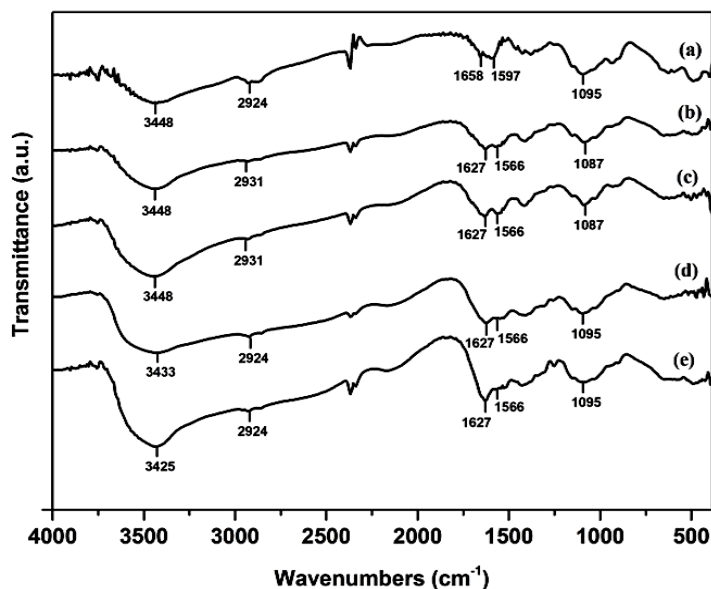
Fig 2. FT-IR spectra of (a) pure chitosan, (b) chitosan/LiI, (c) chitosan/NaI, (d) chitosan/KI, and (e) chitosan/CsI electrolyte systems

obtained from the systems with lower crystallinity. High ionic mobility caused more interaction between I^- and I_3^- in the electrolyte system. As reported previously (Ki *et al.* 2023), the electrolyte's anodic and cathodic peak currents increase with increasing interaction between I^- and I_3^-.

Figure 2 shows the FT-IR spectra of chitosan powder and chitosan-based electrolytes prepared using various iodide salts. A broad absorption at around 3400 cm^{-1} is attributed to –OH and –NH stretching vibration. The absorption at around 2930 cm^{-1} corresponds to the stretching vibration of –CH in the pyranose rings. The band at 1658, 1597, and 1095 cm^{-1} corresponds to the stretching vibration of C=O (amide I), bending vibration of –NH$_2$ (amide II), and stretching vibration of C-O-C bridge, respectively (Karlybaeva *et al.* 2023, Soud *et al.*

2024). An absorption shift is observed at the stretching vibration of –OH and –NH (from 3448 to 3433 and 3425 cm^{-1}), C=O stretching vibration (from 1658 to 1627 cm^{-1}), –NH$_2$ bending vibration (from 1597 to 1566 cm^{-1}), and C-O-C stretching vibration (from 1095 to 1087 cm^{-1}). The interaction of the alkali iodide salts, and the active site groups of the chitosan might cause this shift of stretching and bending vibration to lower energy. The –CH stretching vibration at 2924 cm^{-1} shifts to 2931 cm^{-1}, attributable to the possibility of the formation of M+ and O-C group interactions (Lichawska *et al.* 2019).

The XRD pattern of chitosan and chitosan-based gel electrolytes prepared using various iodide salts is shown in Figure 3. Chitosan (Figure 3a) is partly crystalline with a broad peak at 2θ =10° and 21° due to the intermolecular interaction in

Fig 3: XRD pattern of (a) pure chitosan, (b) chitosan/LiI, (c) chitosan/NaI, (d) chitosan/KI, and (e) chitosan/CsI electrolyte systems

A.D.Hatmanto et al   Int. J. Renew. Energy Dev 2025, 14(4), 727-739

| 731

Table 3

$E_{p/2}$, ΔE_p, and i_{pa}/i_{pc} ratio of gel electrolytes prepared using various iodide salts

| Iodide salts	$E_{p/2}$ (V)	ΔE_p (V)	i_{pa}/i_{pc}
LiI	0.440	0.894	0.999
NaI	0.473	0.969	0.975
KI	0.449	0.950	0.975
CsI	0.453	0.942	0.972
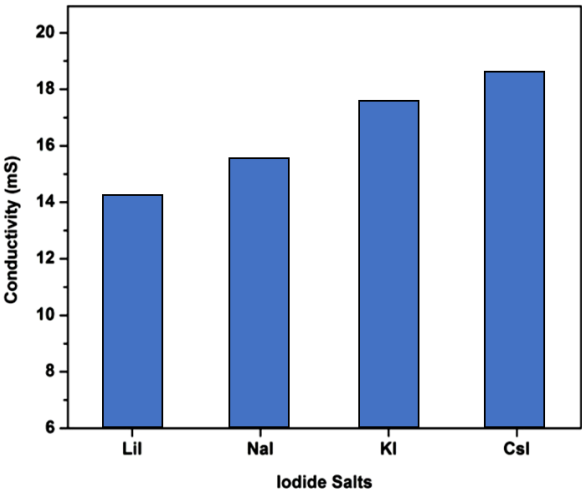
Fig 4. Ionic conductivity of gel electrolytes prepared using various iodide salts

the polymer chains. It can be observed from Figure 3 that the addition of iodide salts can significantly reduce the crystallinity of the chitosan as a matrix, favorable for conductivity improvement. The larger the cation of the alkali iodide salts, the more amorphous electrolyte system can be obtained.

Several parameters related to cyclic voltammetry measurement of gel electrolytes prepared using various iodide salts are then listed in Table 3. The values of half-wave redox potential ($E_{p/2}$) of the electrolyte were relatively constant in different iodide salts. $E_{p/2}$ is a critical parameter related to the regeneration of oxidized dyes in the DSSC systems. Moreover, the ratio of the anodic (oxidation) and cathodic (reduction) peak intensity of the electrolytes is close to 1, suggesting a high reversibility of the I^- oxidation and I_3^- reduction.

Next, we measured the conductivity of the electrolytes prepared in various iodide salts, as presented in Figure 4. The ionic conductivity increases by increasing the cation size of the alkali iodide salts. The highest conductivity of the quasi-solid electrolyte was 18.39 mS, obtained from the electrolyte prepared using CsI (the iodide salt with the largest cation size in the series). This trend of ionic conductivity increment is consistent with the increasing of anodic and cathodic peak currents in Figure 1(b). As reported, the increase in conductivity is usually followed by the rise in redox peak current intensity (Gupta and Rhee 2013), considering the ionic mobility of the redox species involved.

The redox behavior of electrolyte prepared using various iodide salts and the addition of PMII is summarized in Figure 5(a). It shows a strong intensity peak at the voltage range of 0.95 – 1.01 V, attributed to the oxidation of I^-. Meanwhile, the reduction of I_3^- is observed from -0.18 to -0.31 V. Figure 5(b) summarizes the effect of iodide salts and addition of PMII on the redox peak current intensity. PMII introduction increases the redox peak current intensity in all iodide salts. PMII consists of imidazolium cation (PMI$^+$) and iodide anion, providing additional carriers to improve the electrolyte performance. Additionally, PMII acts as a plasticizing agent that dissociates more iodide salts and contributes to the conductivity increase. The ionic conductivity of the quasi-solid electrolytes prepared in different iodide salts with the addition of PMII is shown in Figure 6. It is clear that the addition of PMII can significantly increase the ionic conductivity of the electrolyte. This ionic conductivity increase might be caused by the increasing number of charge carriers due to the plasticizing action of PMII. We considered the electrolyte containing KI and PMII as the
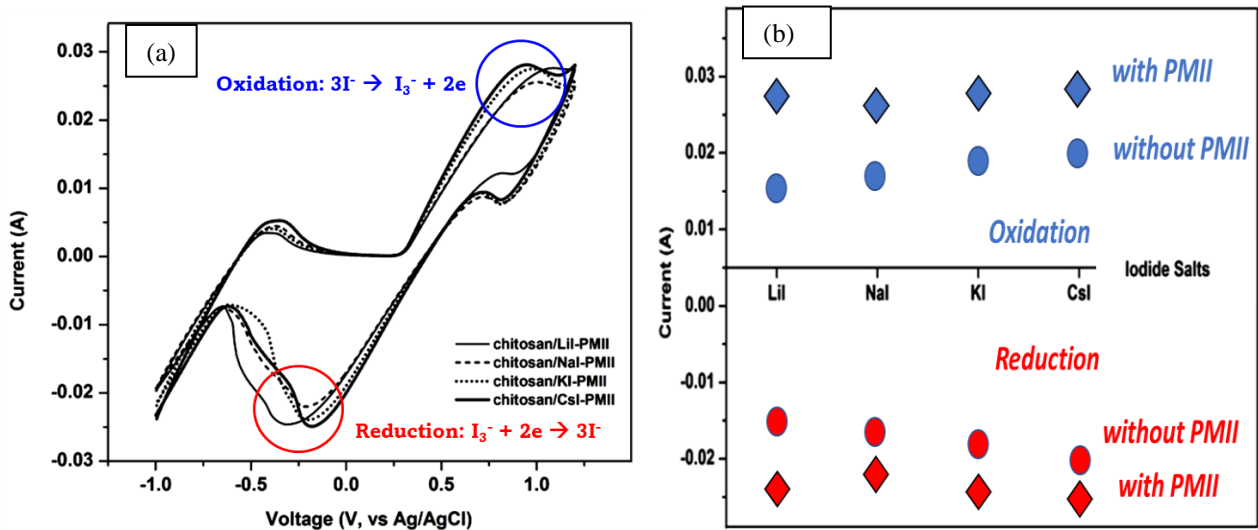
Fig 5. (a) Cyclic voltammograms of gel electrolytes prepared using various iodide salts and the addition of PMII and (b) the effect of iodide salts and addition of PMII on the anodic and cathodic peak current intensity
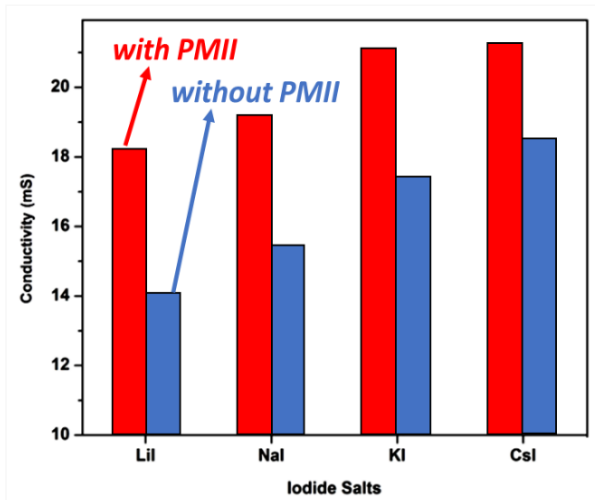
A.D.Hatmanto et al   Int. J. Renew. Energy Dev 2025, 14(4), 727-739

|732

Fig 6. Ionic conductivity of gel electrolytes prepared using various iodide salts and the addition of PMII

Table 4

$E_{p/2}$, ΔE_p, and i_{pa}/i_{pc} ratio of electrolytes prepared at various PMII concentrations

Concentrations of PMII	$E_{p/2}$ (V)	ΔE_p (V)	i_{pa}/i_{pc}
0%	0.443	1.001	1.042
5%	0.434	1.052	1.104
10%	0.409	1.011	1.141
15%	0.396	1.050	1.121
20%	0.385	1.179	1.151

optimized systems since there was no significant conductivity increase by replacing KI with CsI salts.

The redox activity of electrolytes prepared at different amounts of PMII is shown in Figure 7(a). As can be seen, a strong peak is observed in the range of 0.91-0.96 V, attributed to the oxidation of I^-. The reduction of I_3^- was detected at the voltage of -0.06 to -0.20 V. Figure 7(b) showed the effect of concentrations of PMII on the redox current intensity. The current intensity increases parallel with the PMII content. The amount of iodide salts in the electrolyte systems can be dissociated more by employing higher concentrations of PMII, thus resulting in a higher interaction between I^- and I_3^-. The several parameters related to cyclic voltammetry measurement of gel electrolytes prepared at different amounts of PMII are summarized in Table 4. The value of half redox potential of the electrolyte prepared from 20% PMII is observed to be the lowest. The lower $E_{p/2}$ of the electrolyte suggests a larger energy gap between the redox electrolyte and the oxidized dyes, resulting in more thermodynamically spontaneous regeneration. The most extensive peak separation (ΔE_p) was also obtained from the electrolyte containing 20% PMII, indicating a better interaction between the I^- and I_3^- redox couple.
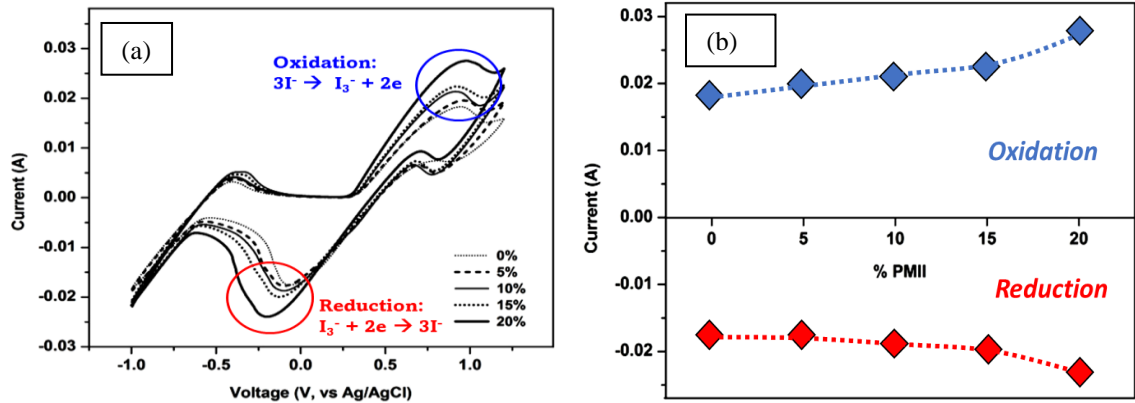
Fig 7. (a) Cyclic voltammograms of gel electrolytes prepared at various concentrations of PMII and (b) the effect of concentrations of PMII on the redox peak current intensity
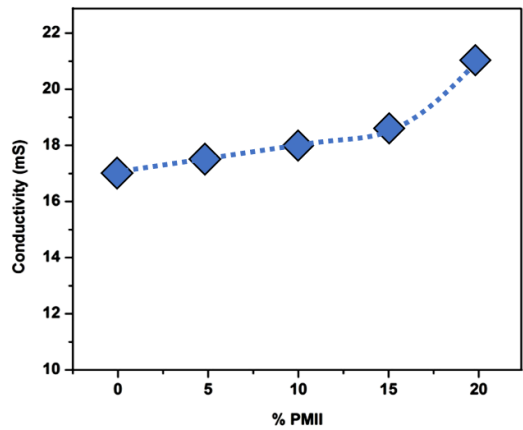
Fig 8. Ionic conductivity of electrolytes prepared at various PMII concentrations

A.D.Hatmanto et al

Int. J. Renew. Energy Dev 2025, 14(4), 727-739

| 733
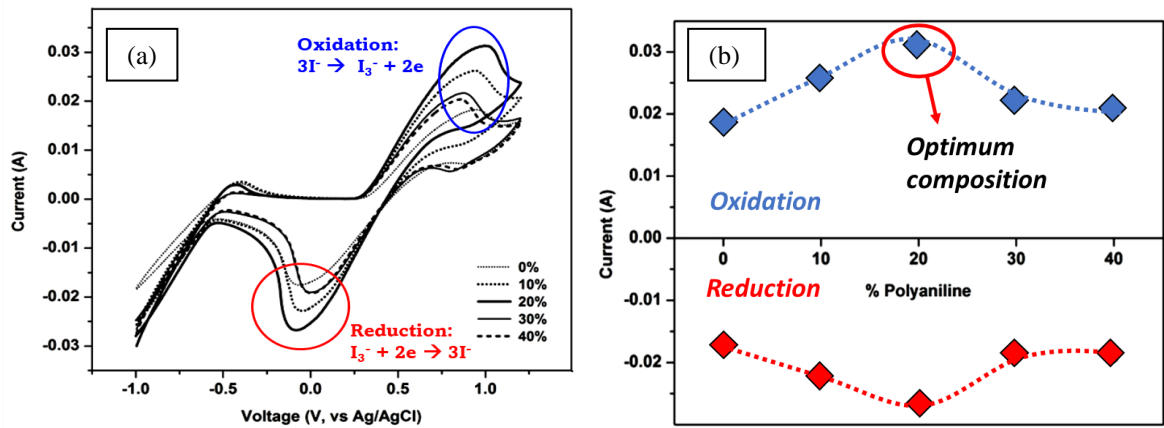
Fig 9. (a) Cyclic voltammograms of gel electrolytes prepared at various concentrations of polyaniline and (b) the effect of concentrations of polyaniline on the anodic and cathodic peak current intensity

The conductivity of quasi-solid electrolytes prepared in different amounts of PMII is presented in Figure 8. The electrolyte's ionic conductivity is higher on electrolytes with higher PMII content. This might be caused by the higher charge carrier mobility in the electrolyte systems due to the plasticizing action of PMII and weaker interaction between PMI$^+$ cation and chitosan matrix. The smaller cation K$^+$ will possibly coordinate stronger to oxygen atoms of chitosan than the larger PMI$^+$ cation. This weak interaction between PMI$^+$ and the active site of chitosan caused PMI$^+$ to move quickly in the electrolyte systems, resulting in a higher ionic conductivity.
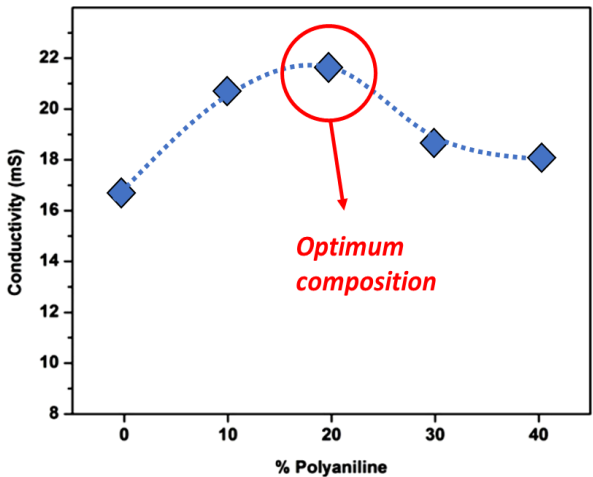
Table 5
$E_{p/2}$, ΔE_p, and i_{pa}/i_{pc} ratio of gel electrolytes prepared at various concentrations of polyaniline

Concentrations of polyaniline	$E_{p/2}$ (V)	ΔE_p (V)	i_{pa}/i_{pc}
0%	0.443	1.001	1.042
10%	0.443	0.996	1.151
20%	0.457	1.079	1.171
30%	0.435	0.874	1.138
40%	0.429	0.852	1.061

Fig 10. Ionic conductivity of gel electrolytes prepared at various concentrations of polyaniline

The electrochemical activity of electrolytes prepared at different amounts of polyaniline is then investigated, as shown in Figure 9(a). A strong intensity peak at 0.86 – 1.00 V indicating the oxidation of I$^-$. The reduction of I$_3^-$ was observed from 0.00 to -0.08 V. Figure 9(b) presents the effect of polyaniline concentrations on the redox peak current intensity. The current intensity increases with increasing concentrations of polyaniline from 0% to 20%, then decreases at 30% and 40%. The increase in redox peak current intensity is possibly caused by the increasing polarity of the polymer matrix due to the existence of conductive polyaniline. Introducing the conductive polyaniline chains into the chitosan matrix also provides additional electron transport pathways, leading to easier electron transport (Tang *et al*. 2012). The decreasing redox peak current intensity at the polyaniline content of 30% and 40% is probably caused by the low solubility of polyaniline in high concentrations, considering the inhomogeneity of those electrolyte systems. Several parameters to interpret the results of cyclic voltammetry measurement of gel electrolytes prepared at various concentrations of polyaniline are listed in Table 5. As indicated, the values of half redox potential ($E_{p/2}$) of the electrolytes prepared at different concentrations of polyaniline were relatively constant. The largest peak separation (ΔE_p) was obtained from the electrolyte containing 20% polyaniline, indicating high I$^-$ and I$_3^-$ redox pair interaction.

The conductivity of electrolytes prepared in different amounts of polyaniline is shown in Figure 10. It increases with increasing concentrations of polyaniline from 0% to 20%, then decreases at 30% and 40%, consistent with the trend of increasing anodic and cathodic peak current intensity in Figure 9.b. As mentioned before, this ionic conductivity improvement might be induced by the higher polarity of the polymer matrix with conductive polyaniline. The higher the polarity of the matrix, the more iodide salts can be dissociated, resulting in a higher charge carriers, and increasing the electrolyte's conductivity. The low solubility of polyaniline in higher concentrations may block the movement of the ions and lower the conductivity.

The chitosan-based quasi-solid electrolyte showing the best performance in each study was then employed in a DSSC system. The electrochemical activity of chitosan-based gel electrolytes prepared at various compositions is shown in Figure 11(a). The oxidation of I$^-$ was observed at the voltage of 0.94 – 1.02 V, while the I$_3^-$ reduction was detected in the range of -0.06 to -0.20 V. Figure 11(b) shows the influence of the

A.D.Hatmanto et al

Int. J. Renew. Energy Dev 2025, 14(4), 727-739

| 734

Table 6

$E_{p/2}$, ΔE_p, and i_{pa}/i_{pc} ratio of gel electrolytes prepared at various compositions of polymer matrix and electrolyte

| Composition	$E_{p/2}$ (V)	ΔE_p (V)	i_{pa}/i_{pc}
chitosan/KI	0.443	1.001	1.042
chitosan/KI-PMII	0.385	1.179	1.151
chitosan-polyaniline/KI	0.466	1.101	1.210
chitosan-polyaniline/KI-PMII	0.404	1.084	1.180
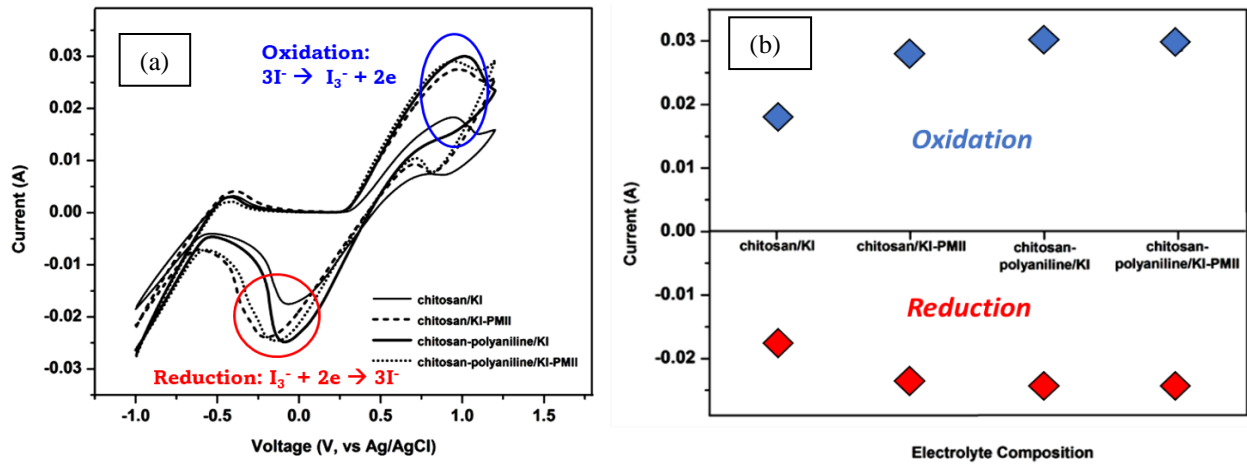
Fig 11.. a) Cyclic voltammograms of gel electrolytes prepared at various compositions and (b) the effect of electrolyte composition on the redox peak current intensity

composition of polymer matrix and electrolyte on the redox peak current intensity. It increases with the use of PMII, polyaniline, or a combination of PMII-polyaniline. The anodic peak current intensity increases from 0.018 A to 0.028-0.030 A, while the cathodic peak current increases from -0.018 A to -0.025 A. The detailed parameters related to cyclic voltammetry measurement of gel electrolytes are listed in Table 6.

The electrolyte's conductivity of prepared in various compositions of polymer matrix and electrolyte is presented in Figure 12(a). The conductivity increases with the use of PMII, polyaniline, or a combination of PMII-polyaniline, consistent with the results of cyclic voltammetry evaluation. Conductivity increases from 17.09 mS to 21.01-21.57 mS. There is no significant enhancement by combining PMII and polyaniline in

both the anodic-cathodic peak current and electrolyte's conductivity compared to electrolyte containing only PMII or polyaniline alone.

Another crucial characteristic of quasi-solid electrolytes is their stability under light irradiation. To evaluate the stability of the chitosan-based electrolyte under visible light exposure, we irradiated 30 mL of chitosan-based gel electrolyte (placed in a 50 mL-beaker glass) using a 500 W visible light for 60, 90, and 120 min, while the lamp is positioned about 20 cm above the sample. The exposed surface area is estimated to receive about 6.9 W of power, considering the estimated irradiance at this distance, that is approximately 5000 W/m². Such exposures for 60, 90, and 120 min correspond to roughly 12.5, 18.8, and 25 h of sunlight irradiation, respectively. As indicated from the CV
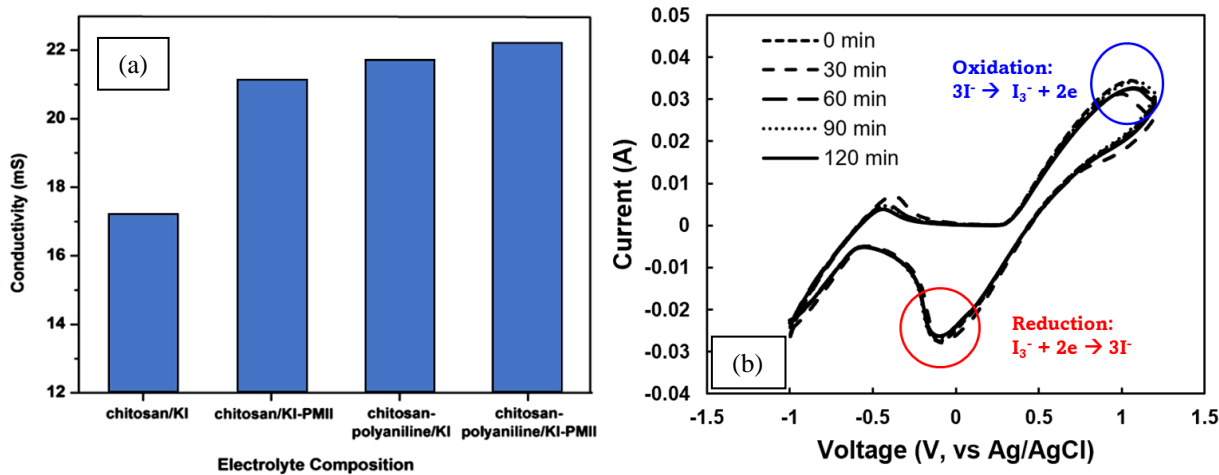
Fig 12. (a) Ionic conductivity of electrolytes prepared at various electrolyte compositions and (b) stability of electrolytes under visible light irradiation at a power of 500 W, with the light source positioned 20 cm away.

A.D.Hatmanto et al

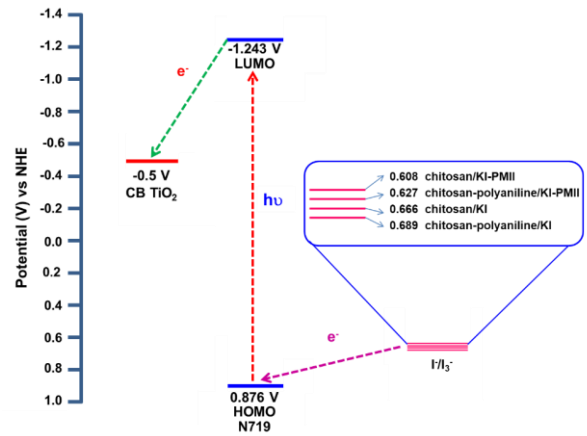Int. J. Renew. Energy Dev 2025, 14(4), 727-739

| 735
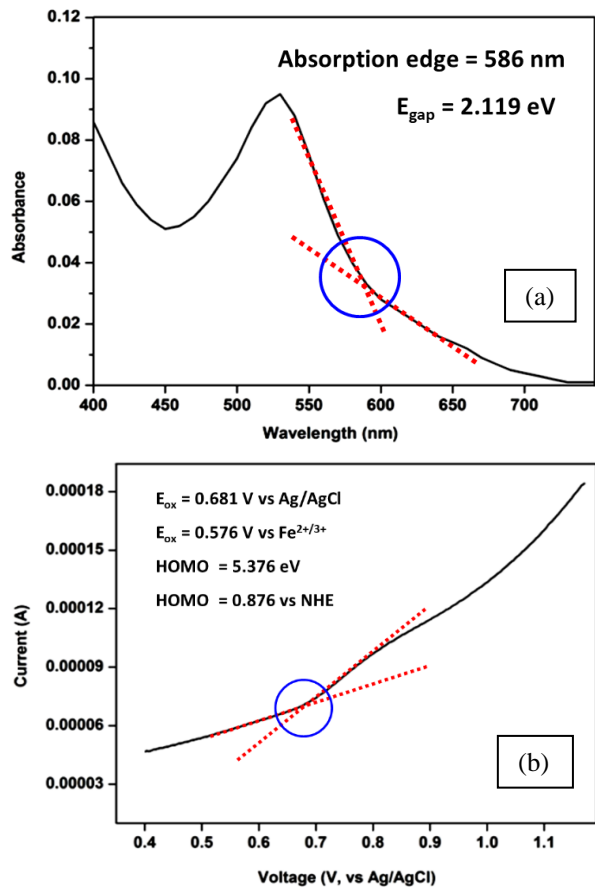
Fig 13. (a) UV-Vis absorption spectrum and (b) cyclic voltammogram of N719 dye. The absorption edge of 586 nm equals to 2.119 eV energy gap, while onset anodic potential of 0.681 V (vs. Ag/AgCl) corresponds to HOMO energy level of 0.876 V (vs. NHE).
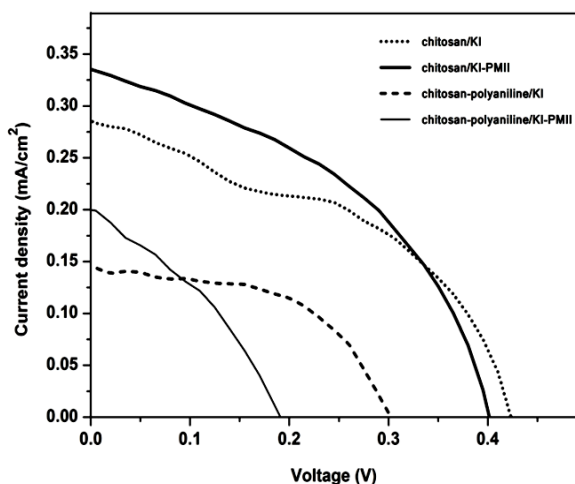

Fig 14: Schematic energy level diagram of chitosan electrolyte-based DSSC using various compositions of redox electrolyte. All values have been converted to potentials relative to the NHE. The LUMO level of the N719 dye was calculated by subtracting its bandgap energy from the HOMO level (see Fig. 13). The conduction band edge of TiO_2 is −0.74 V (vs. standard calomel electrode, SCE) (Zanotti et al., 2010), equivalent to approximately -0.50 V vs. NHE.

analysis results in Fig. 12(b), the gel electrolyte maintained its electrochemical performance after all exposure durations, indicating good stability under prolonged visible light irradiation. In contrast, the stability of ethylene glycol-based liquid electrolyte under the same conditions is significantly lower. We found that the solvent in the liquid electrolyte is completely evaporated within a few minutes, indicating its poor stability against visible light exposure, that at the same time, may also generate heat. This heat generation can also accelerate the evaporation process in liquid systems.

Then, we fabricated a quasi-solid DSSC using those optimized chitosan-based electrolyte systems. For the working electrode, a conventional N719 dye was used as a photosensitizer for an ITO transparent conductive glass coated with nanocrystalline TiO_2. The UV-Vis absorption of N719 dyes is presented in Figure 13(a) and used to determine its band gap energy. It showed a strong peak at 529 nm. Meanwhile, the band gap energy is calculated based on the absorption, which is the cross-section of the absorption baseline and the initial absorption increment (Shafiee et al. 2011). The absorption edge is observed at 586 nm, corresponding to the energy gap of 2.119 eV (see the blue circle in Fig. 13(a)).

Cyclic voltammetry (shown in Figure 13(b)) was then used to determine the HOMO energy level of N719 dyes and create a schematic illustration of energy level diagram of electron flow in DSSC. It shows a low-intensity oxidation peak observed at around 0.8 V, attributed to the electrochemical activity of N719. The HOMO level of N719 was calculated based on the onset

anodic potential, a cross-section of the baseline and the anodic peak (Shafiee et al. 2011). Pair of $Fe(CN)_6^{4-}/Fe(CN)_6^{3-}$ is used as an external standard. From Figure 13(b), the onset anodic potential was observed at 0.681 V (see the blue circle). The LUMO energy level was then calculated from the band gap energy and the HOMO energy level of the N719 dye. The HOMO and LUMO energy levels of the N719 dyes were 0.876 and -1.243 V (vs. normal hydrogen electrode (NHE)), respectively. The HOMO level energy obtained in this study is similar to the HOMO level of N719 previously reported (Zhang et al. 2014), that is 0.870 V (vs. NHE).

Figure 14 represents the schematic illustration of N719-sensitized DSSC leveling energy diagram, employed I^-/I_3^- as redox electrolytes. Figure 14 confirms the LUMO of N719 dyes (-1.243 V vs. NHE) is more negative than the conduction band (CB) of TiO_2 (-0.5 V vs. NHE) (Zanotti et al., 2010), which ensures the required driving force for injection of electrons to the CB of TiO_2 semiconductor from the excited state of the dye (Wu et al. 2010, Kim et al. 2013, Jolly et al. 2014). The HOMO energy level of N719 (0.876 V vs. NHE) was found to be more positive compared to the half-wave redox potential of I^-/I_3^- (0.608-0.689 V vs. NHE), suggesting that the electron from I^- can be thermodynamically transferred to the oxidized state of N719. The oxidized N719 photosensitizer can be regenerated if the HOMO energy is more positive than $E_{p/2}$ of the I^-/I_3^- pair. Therefore, in this DSSC system, the oxidized N719 can be

Table 7
Photovoltaic performance of DSSC prepared at various compositions of electrolyte

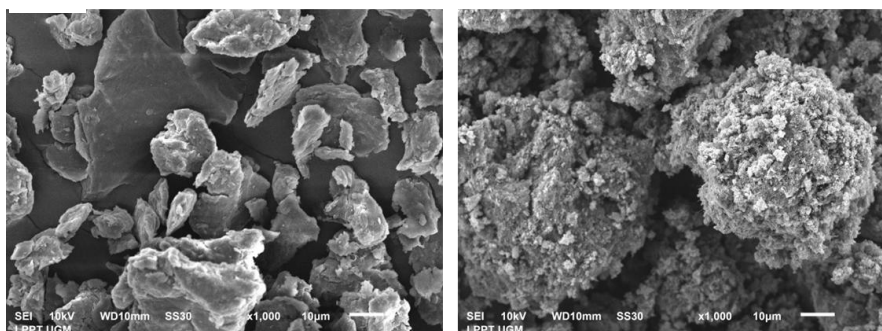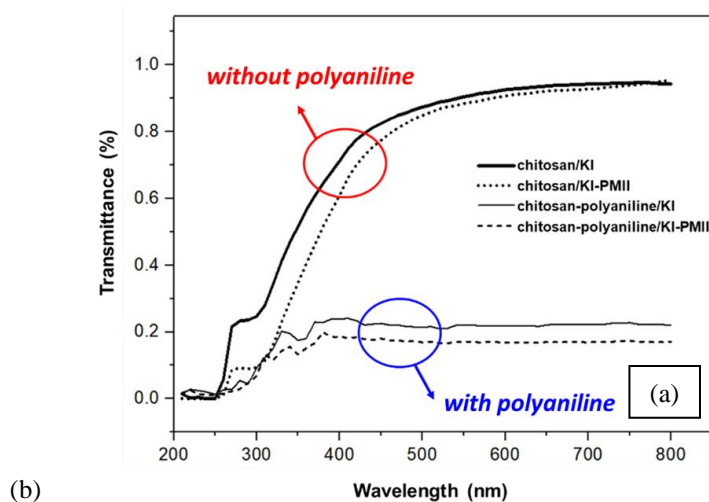| Composition	V_{oc} (V)	J_{sc} (mA/cm^2)	FF	η (%)
acetonitrile/KI (liquid)	0.470	1.307	0.330	0.203
chitosan/KI	0.424	0.287	0.434	0.053
chitosan/KI-PMII	0.402	0.335	0.432	0.058
chitosan-polyaniline/KI	0.301	0.144	0.531	0.023
chitosan-polyaniline/KI-PMII	0.191	0.200	0.350	0.013

A.D.Hatmanto et al

Int. J. Renew. Energy Dev 2025, 14(4), 727-739

|736

Fig 15: Photovoltaic performance of the DSSC fabricated using chitosan-based gel electrolyte prepared at various compositions

density (J_{sc}), fill factor (FF), and the overall power conversion efficiency (η). DSSC prepared from PMII-based chitosan electrolyte systems shows higher Jsc and lower V_{oc}. It might be caused by the adsorption of K^+ in the PMII-based electrolyte system, which is more than the non-PMII-based system, due to the plasticizing action of PMII. Cation adsorption on the surface of TiO_2 causes the CB of TiO_2 to shift positively and is associated with the drop in V_{oc} and an increase in J_{sc} of DSSC. This positive shift also supports the driving force for the injection of charge from the excited N719 to TiO_2, providing a higher photocurrent density of the DSSC (Dissanayake *et al.* 2014). The best performance was obtained from DSSC prepared from a chitosan/KI-PMII electrolyte system that showed V_{oc} of 0.402 V, J_{sc} of 0.335 mA/cm^2, FF of 0.432 and overall power conversion efficiency (PCE) of 0.058%. This result is comparable to the value reported by Yahya *et al.* (2020), who used tripropyl chitosan as the electrolyte matrix and achieved conversion efficiency of 0.075%. It was further enhanced to 0.415% with the incorporation of an ionic liquid. Our results are also in good agreement with Buraidah *et al.* (2016), who achieved power conversion efficiencies of 0.06% using red cabbage dye and improved to 0.78% using N3 dye, both employing a chitosan/PEO electrolyte matrix in their DSSC fabrication. Due to limited availability of our working electrode and the counter electrode, only one device could be fabricated and tested per electrolyte. As a result, error margins or standard deviations could not be determined. While the results provide a useful comparative overview, further testing with multiple devices is required to confirm reproducibility and evaluate performance variability.

theoretically regenerated by the I$^-$/I$_3^-$ couple in all electrolyte compositions.

The photovoltaic test of the DSSC fabricated using chitosan-based gel electrolyte in various compositions and N719 photosensitizer is shown in Figure 15. For comparison, a conventional DSSC using acetonitrile as liquid electrolyte was also measured. The photovoltaic performances of DSSC were evaluated based on several parameters (summarized in Table 7), they are open circuit voltage (V_{oc}), short circuit current

Fig 16. (a) UV-Vis spectra of the chitosan-based gel electrolyte prepared with and without polyaniline. SEM images of (b) chitosan and (c) polyaniline with 1000× magnification.

A.D.Hatmanto et al

Int. J. Renew. Energy Dev 2025, 14(4), 727-739

| 737

The relatively low DSSC's efficiency prepared using a chitosan-polyaniline electrolyte system is possibly caused by the decreasing transparency of the gel electrolyte system (see Fig. 16(a)), considering the low transmittance of the UV-Vis spectrum of the samples containing polyaniline. In our case, we predict the negative impact of polyaniline incorporation may be attributed to its large particle size. SEM analysis (Fig.16(b-c)) indicated a significant aggregation of polyaniline, with overall particle sizes ranging from 50–60 μm. On the other hand, chitosan has a smaller size ranging from 10–30 μm. Different from polyaniline that show inhomogenous dispersion in the mixture, particularly at higher concentrations (above 20% w/w, see Fig.9), chitosan dissolved perfectly in 1% acetic acid. This poor dispersion of polyaniline likely hinders the ionic movement and limits the overall I^-/I_3^- redox reaction. In addition, the relatively larger particle size and aggregation contributes to the reduced transparency of the electrolyte, thus limiting light penetration into the systems. Future works should optimize the particle size of polyaniline, especially to the nanoscale, to improve its dispersion in the matrix, enhance the I^-/I_3^- redox cycle, and improve the overall power conversion efficiencies.

The development of eco-friendly DSSCs can be further advanced by integrating polyaniline and ionic liquids with nanoparticles (Pullanjiot and Swaminathan, 2019; Hidayat *et al.*, 2024; Solikah *et al.*, 2024). The synergistic combination of conducting polymers and nanofillers not only enhances the amorphousness of the matrix (favoring improved ionic conductivity), but also significantly strengthens the mechanical properties of the polymer composite. This promising approach paves the way for further innovation in biopolymer-based electrolytes, contributing to the advancement of sustainable and environmentally friendly DSSCs.

4. Conclusion

This work focused on the design and characterization of chitosan as a polymer matrix for I^-/I_3^- redox electrolyte and its performance enhancement by polyaniline and ionic liquid introduction to be employed in DSSCs. The chitosan-based quasi-solid electrolyte prepared from iodide salts with the larger cation size showed higher conductivity and redox current intensity due to the increasing amorphousness of the electrolyte systems. The conductivity and redox current intensity also increased with the concentration of PMII due to increasing dissociated iodide salts and ionic mobility. Polyaniline improved the electrolyte redox activities, but the DSSC showed lower conversion efficiency due to its decreasing electrolyte transparency. Our results show that chitosan can be considered a promising biopolymer for an environmentally friendly and low-cost quasi-solid-state DSSC.

Acknowledgments

Author Contributions: ADH: Conceptualization, Methodology, Formal Analysis, Writing-Original Draft. IP: Formal Analysis, Visualization, YNKT: Formal Analysis, Visualization, SJS: Supervision, Writing-Review and Editing. IK: Conceptualization, Supervision, Writing-Review and Editing.

Conflicts of Interest: The authors declare no conflict of interest.

References

Adel, R., Abdallah ,T., and Talaat, H. (2019). Efficiency enhancement of photovoltaic performance of dye sensitized solar cell using conducting polymer electrolyte of different functional group. *Journal of Physics: Conference Series*, 1253 (1), 012029. https://doi.org/10.1088/1742-6596/1253/1/012029

Arof, A.K., Aziz, M.F., Noor, M.M., Careem, M.A., Bandara, L.R.A.K., Thotawatthage, C.A., Rupasinghe, W.N.S., and Dissanayake, M.A.K.L. (2014). Efficiency enhancement by mixed cation effect in dye-sensitized solar cells with a PVdF based gel polymer electrolyte. *International Journal of Hydrogen Energy*, 39, 2929 – 2935. https://doi.org/10.1016/j.ijhydene.2013.07.028

Bandara, T.M.W.J., DeSilva, L.A.A., Ratnasekera, J.L., Hettiarachchi, K.H., Wijerathna, A.P., Thakurdesai, M., Preston, J., Albinsson, I., and Mellander, B.E. (2019). High Efficiency Dye-Sensitized Solar Cell Based on a Novel Gel Polymer Electrolyte Containing RbI and Tetrahexylammonium Iodide (Hex4NI) Salts and Multi-Layered Photoelectrodes of TiO_2 Nanoparticles. *Renewable Sustainable Energy Rev.* 103, 282-290. https://doi.org/10.1016/j.rser.2018.12.052

Bhattacharya, B., Lee, J.Y., Geng, J., Jung, H.T., and Park, J.K. (2009). Effect of cation size on solid polymer electrolyte based dye-sensitized solar cells. Langmuir, 25, 3276-3281. https://doi.org/10.1021/la8029177

Buraidah, M.H., Teo, L.P., Au Yong, C.M., Shah, S., and Arof, A.K. (2016) Performance of polymer electrolyte based on chitosan blended with poly(ethylene oxide) for plasmonic dye-sensitized solar cell. *Optical Materials*, 57, 202-211. https://doi.org/10.1016/j.optmat.2016.04.028

Buraidah, M.H., Teo, L.P., Majid, S.R., and Arof, A.K. (2010). Characteristics of TiO_2/solid electrolyte junction solar cells with I/I_3^- redox couple. *Optical Materials,* 32, 723 – 728. https://doi.org/10.1016/j.optmat.2009.08.014

Dissanayake, M.A.K.L., Jayathissa, R., Seneviratne, V.A., Thotawatthage, C.A., Senadeera, G.K.R., and Mellander, B.E. (2014). Polymethylmethacrylate (PMMA) based quasi-solid state electrolyte with binary iodide salt for efficiency enhancement in TiO_2 based dye sensitized solar cells. *Solid State Ionics*, 265, 85-91. https://doi.org/10.1016/j.ssi.2014.07.019

Gossen, K., Dotter, M., Brockhagen, B., Storck, J.L., and Ehrmann, A. (2022). Long-term investigation of unsealed DSSCs with glycerol-based electrolytes of different compositions. *AIMS Materials Science,* 9 (2), 283-296. https://doi.org/10.3934/matersci.2022017

Green, M.A., Hishikawa, Y., Warta, W., Dunlop, E.D., Levi, D.H., Hohl-Ebinger, J., and Ho-Baillie, A.W.H. (2017). Solar Cell Efficiency Tables (Version 50). Prog. *Photovoltaics*, 25, 668-676. https://doi.org/10.1002/pip.2909

Gupta R.K., and Rhee H.-W. (2013). Plasticizing effect of K^+ ions and succinonitrile on electrical conductivity of [poly(ethylene oxide)-succinonitrile]/KI-I_2 redox-couple solid polymer electrolyte. *Journal of Physical Chemistry B,* 117 (24), 7465 - 7471. https://doi.org/10.1021/jp4025798

Hidayat, A., Solikah, S., Shafa, A.V.A., and Hatmanto, A.D. (2024). Hypothetical introduction of TiO_2 nanodecahedrons (TN(10)) as the design for quasi solid dye sensitized solar cells based on KI-I_2/chitosan/PAni-chitosan/TN(10) by the p-n junction theory. *Electrochimica Acta,* 477, 143740. https://doi.org/10.1016/j.electacta.2023.143740

Huang, Y.-J., Sahoo, P.K., Tsai, D.-S., and Lee, C.-P. (2021). Recent advances on pt-free electro-catalysts for dye-sensitized solar cells. *Molecules,* 26 (17), 5186. https://doi.org/10.3390/molecules26175186

Jolly, D., Pelleja, L., Narbey, S., Oswald, F., Chiron, J., Clifford, J., Palomares, E., and Demadrille, R. (2014). Robust organic dye for dye sensitized solar cells based on iodine/iodide electrolytes combining high efficiency and outstanding stability. *Scientific Reports,* 4 (4033), 1-7. https://doi.org/10.1038/srep04033

Kaneto, K., Hata, F., Uto, S. (2018). Structure and size of ions electrochemically doped in conducting polymer. Journal of

A.D.Hatmanto et al

Int. J. Renew. Energy Dev 2025, 14(4), 727-739

| 738

Micromechanics and Microengineering, 28 (5), 054003. https://doi.org/10.1088/1361-6439/aaaef5

Karlybaeva, B.P., Berdimbetova, G.E., Boymirzaev, A.S. (2023). Synthesis and characteristics of sulfated chitosan based on chitin/chitosan from artemia parthenogenetica cysts. *Chemical Problems*, 3 (21), 242-250. https://doi.org/10.32737/2221-8688-2023-3-242-250

Ki S., Park A., Lee W.B., Kim, Y.J., and Chang J. (2023). Overlimiting current by iodide electrode oxidation in aqueous media: an electrogenerated iodine interphase with positively charged channels stimulating in situ electrokinetic iodide transport. *Journal of Materials Chemistry A,* 11 (26), 14366-14379. https://doi.org/10.1039/D3TA01505J

Kim, S.G., Ju, M.J., Choi, I.T., Choi, W.S., Choi, H.J., Baek, J.B., and Kim, H.K. (2013). Nb-doped TiO2 nanoparticles for organic dye-sensitized solar cells. *RSC Advances,* 3 (37), 16380 - 16386. https://doi.org/10.1039/C3RA42081G

Kitazawa, Y., Iwata, K., Kido, R., Imaizumi, S., Tsuzuki, S., Shinoda, W., Ueno, K., Mandai, T., Kokubo, H., Dokko, K., and Watanabe, M. (2018). Polymer Electrolytes Containing Solvate Ionic Liquids: A New Approach to Achieve High Ionic Conductivity, Thermal Stability, and a Wide Potential Window. *Chem. Mater.* 30, 252-261. https://doi.org/10.1021/acs.chemmater.7b04274

Kusumawati, N., Setiarso, P., Muslim, S., Hafidha, Q.A., Cahyani, S.A., and Fachrirakarsie, F.F. (2024). Optimization Thickness of Photoanode Layer and Membrane as Electrolyte Trapping Medium for Improvement Dye-Sensitized Solar Cell Performance. *Science and Technology Indonesia,* 9 (1), 7-16. https://doi.org/10.26554/sti.2024.9.1.7-16

Lai Y.-L., Hsu H.-R., Lai Y.-K., Zheng, C.-Y, Chou, Y.-H., Hsu, N.-K., and Lung G.-Y. (2017). Influence of thin film thickness of working electrodes on photovoltaic characteristics of dye-sensitized solar cells. *MATEC Web of Conferences*, 123, 00030. https://doi.org/10.1051/matecconf/201712300030

Lemos, H.G., Barba, D., Selopal, G.S., Wang, C., Wang, Z.M., Duong, A., Rosei, F., Santos, S.F., and Venancio, E.C. (2020). Water-dispersible polyaniline/graphene oxide counter electrodes for dye-sensitized solar cells: Influence of synthesis route on the device performance. *Sol. Energy,* 207, 1202-1213. https://doi.org/10.1016/j.solener.2020.07.021

Li, G.B., Wang, J., Kong, X.P. (2020). Coprecipitation-based synchronous pesticide encapsulation with chitosan for controlled spinosad release. *Carbohydr. Polym.,* 249, 116865. https://doi.org/10.1016/j.carbpol.2020.116865

Lichawska, M.E., Kufelnicki A., Wozniczka, M. (2019). Interaction of microcrystalline chitosan with graphene oxide (GO) and magnesium ions in aqueous solution. *BMC Chemistry*, 13 (3), 57. https://doi.org/10.1186/s13065-019-0574-y

Liu, G., Hu, M., Du, X., Qi, B., Lu, K., Zhou, S., Xie, F., and Li, Y. (2022). Study on the interaction between succinylated soy protein isolate and chitosan and its utilization in the development of oil-in-water bilayer emulsions. *Food Hydrocoll.,* 124, 107309. https://doi.org/10.1016/j.foodhyd.2021.107309

Lozkins, S., Hodakovska, J., Kleperis, J., and Merijs-Meri, R. (2019). Nafion® and polyaniline composite modification with Li and Mg ions. *IOP Conference Series: Materials Science and Engineering*, 503 (1), 012031. https://doi.org/10.1088/1757-899X/503/1/012031

Mahmood, H., Shakeel, A., Rafique, S., and Moniruzzaman, M. (2022). Recent progress in ionic liquid-assisted processing and extraction of biopolymers. *Biocatalysis in Green Solvents*, 233-255. https://doi.org/10.1016/B978-0-323-91306-5.00015-7

Manikandan, K.M., Yelilarasi, A., Senthamaraikannan, P., Saravanakumar, S.S., Khan, A., and Asiri, A.M. (2018). The conducting polymer electrolyte based on polypyrrole-polyvinyl alcohol and its application in low-cost quasi-solid-state dye-sensitized solar cells. *J. Solid State Electr.*, 22, 3785-3797. https://doi.org/10.1007/s10008-018-4070-4

O'Regan, B., and Gratzel, M. (1991). A low-cost, high-efficiency solar cell based on dye-sensitized colloidal TiO₂ films. *Nature,* 353 (6346), 737-740. http://dx.doi.org/10.1038/353737a0

Polesca, C., Passos, H., Coutinho, J.A.P., and Freire, M.G. (2022). Sustainable development of biomaterials using ionic liquids. *Current Opinion in Green and Sustainable Chemistry*, 37, 100675. https://doi.org/10.1016/j.cogsc.2022.100675

Prabakaran, K., Mohanty, S., and Nayak, S.K. (2015). Improved electrochemical and photovoltaic performance of dye sensitized solar cells based on PEO/PVdF-HFP/silane modified TiO₂ electrolytes and MWNCT/Nafion counter electrode. *RSC Advances,* 5, 40491-40504. https://doi.org/10.1039/C5RA01770J

Pullanjiot, N., and Swaminathan, S. (2019). Enhanced electrochemical properties of metal oxide interspersed polymer gel electrolyte for QSDSSC application. *Sol. Energy,* 186, 37–45. https://doi.org/10.1016/j.solener.2019.04.086

Senevirathne, A.M.C., Seneviratne, V.A., Ileperuma, O.A., Bandara, H.M.N., and Rajapakse, R.M.G. (2016). Novel Quasi-Solid-State Electrolyte Based on γ-Butyrolactone and Tetrapropylammonium Iodide for Dye-Sensitized Solar Cells Using Fumed Silica as the Gelling Agent. *Procedia Engineering*, 139, 87-92. https://doi.org/10.1016/j.proeng.2015.08.1117

Shafiee, A., Salleh, M.M., and Yahaya, M. (2011). Determination of HOMO and LUMO of [6,6]-phenyl C61-butyric acid 3-ethylthiophene ester and poly(3-octyl-thiophene-3,5-diyl) through voltammetry characterization. *Sains Malaysiana*, 40(2), 173-176.

Singh, P.K., Bhattacharya, B., Nagarale, R.K., Kim, K.W., and Rhee, H.W. (2010). Synthesis, characterization and application of biopolymer-ionic liquid composite membranes. *Synthetic Metal*s, 160, 139 – 142. https://doi.org/10.1016/j.synthmet.2009.10.021

Solikah, S., Hidayat, A., Suyanta, S., and Hatmanto, A.D. (2024). Crystalline phase dependence of the electrochemical properties of chitosan/polyaniline/TiO₂-KI/I₂ quasi solid polymer electrolyte. Materials Science and Engineering B, 307, 117531. https://doi.org/10.1016/j.mseb.2024.117531

Soud, S.A., Ali, M.A., Alhadban, W.G., and Taha, A.A. (2024). Extraction and characterization of chitin and chitosan from local Iraqi fish scales. *Iraqi Journal of Agricultural Sciences*, 55 (5), 1728-1733. https://doi.org/10.36103/1zah0b15

Tamilselvan, S.N., Shanmugan, S., (2024). Towards sustainable solar cells: unveiling the latest developments in bio-nano materials for enhanced DSSC efficiency. *Clean Energy*. 8 (3), 238-257. https://doi.org/10.1093/ce/zkae031

Tang, Z.,Wu, J., Liu, Q., Zheng, M., Tang, Q., Lan, Z., and Lin, J. (2012). Preparation of poly(acrylic acid)/gelatin/polyaniline gel-electrolyte and its application in quasi-sloid state dye sensitized solar cells. *Journal of Power Sources,* 203, 282-287. https://doi.org/10.1016/j.jpowsour.2011.11.039

Theerthagiri, J., Senthil, R.A., Buraidah, M.H., Madhavan, J., Arof, A.K., and Ashokkumar, M. (2016). One-step Electrochemical Deposition of Ni1–xMoxS Ternary Sulfides as an Efficient Counter Electrode for Dye-sensitized Solar Cells. *J. Mater. Chem.,* 4, 16119-16127. https://doi.org/10.1039/C6TA04405K

Vimala, V., Cindrella, L. (2022). Binder-free polymer material embedded in chitosan matrix for electrochemical energy storage devices. *Chemical Physics Letters,* 809, 140172. https://doi.org/10.1016/j.cplett.2022.140172

Wang, X., Kulkarni, S.A., Ito, B.I., Batabyal S.K., Nonomura, K., Wong, C.C., Gratzel, M., Mhaisalkar, S.G., and Uchida, S. (2013). Nanoclay Gelation Approach toward Improved Dye-Sensitized Solar Cell Efficiencies: An Investigation of Charge Transport and Shift in the TiO₂ Conduction Band. *ACS Applied Materials & Interfaces*, 5 (2), 444-450. https://doi.org/10.1021/am3025454

Wu, T.Y., Tsao, M.H., Chen, F.L., Su, S.G., Chang, C.W., Wang, H.P., Lin, Y.C., and Sun, I.W. (2010). Synthesis and characterization of three organic dyes with various donors and rhodamine ring acceptor for using in dye-sensitized solar cells. *Journal of The Iranian Chemical Society*, 7(3), 707-720. https://doi.org/10.1007/BF03246061

Yahya, W.Z.N., Hong, P.Z., Zain, W.Z.Z.W.M., and Mohamed, N.M. (2020). Tripropyl Chitosan iodide-based gel polymer electrolyte as quasi solid-state dye sensitized solar cells. *Materials Science Forum,* 997, 69-76. https://doi.org/10.4028/www.scientific.net/MSF.997.69

Yahya, W.Z.N., Meng, W.T., Khatani, M., Samsudin, A.E., and Mohamed, N.M. (2017). Bio-based chitosan/PVdF-HFP polymer-blend for quasi-solid state electrolyte dye-sensitized solar cells. *e-Polymers*, 17(5), 355-361. https://doi.org/10.1515/epoly-2016-0305

Zanotti, G., Angelini, N., Notarantonio, S., Paoletti, A.M., Pennesi, G., Rossi, G., Lembo, A., Colonna, D., Di Carlo, A., Reale, A., Brown,

A.D.Hatmanto et al   Int. J. Renew. Energy Dev 2025, 14(4), 727-739

| 739

T.M., and Calogero G. (2010). Bridged Phthalocyanine Systems for Sensitization of Nanocrystalline TiO₂ Films. *International Journal of Photoenergy,* 136807, 1-11. https://doi.org/10.1155/2010/136807

Zhang, J., Yu, C., Wang, L., Li, Y., Ren, Y., and Shum, K. (2014). Energy barrier at the N719-dye/CsSnI3 interface for photogenerated holes in dye-sensitized solar cells. *Scientific Reports*, 4(6954), 1-6. https://doi.org/10.1038/srep06954

Zhang, W., Tao, L., Wang, H., and Zhang, J. (2018). Research Progress on Quasi-Solid-State Electrolytes of Dye-Sensitized Solar Cells. *Materials China*. 37 (7), 543-550. https://doi.org/10.7502/j.issn.1674-3962.2018.07.07